THE
EMBO
JOURNAL

Autophagy proteins control goblet cell function by potentiating reactive oxygen species production

Khushbu K Patel[1], Hiroyuki Miyoshi[1],
Wandy L Beatty[2], Richard D Head[3],
Nicole P Malvin[1], Ken Cadwell[4],
Jun-Lin Guan[5], Tatsuya Saitoh[6],
Shizuo Akira[6], Per O Seglen[7],
Mary C Dinauer[1,8], Herbert W Virgin[1]
and Thaddeus S Stappenbeck[1,*]

[1]Department of Pathology and Immunology, Washington University School of Medicine, St Louis, MO, USA, [2]Department of Molecular Microbiology, Washington University School of Medicine, St Louis, MO, USA, [3]Department of Genetics, Washington University School of Medicine, St Louis, MO, USA, [4]Department of Microbiology, Skirball Institute, New York University School of Medicine, New York, NY, USA, [5]Division of Molecular Medicine and Genetics, Department of Internal Medicine, University of Michigan Medical School, Ann Arbor, MI, USA, [6]Laboratory of Host Defense, WPI Immunology Frontier Research Center, Osaka University, Osaka, Japan, [7]Prostate Cancer Research Group, Centre for Molecular Medicine Norway, Nordic EMBL Partnership, University of Oslo and Oslo University Hospital, Oslo, Norway and [8]Department of Pediatrics. Washington University School of Medicine, St Louis, MO, USA

Delivery of granule contents to epithelial surfaces by secretory cells is a critical physiologic process. In the intestine, goblet cells secrete mucus that is required for homeostasis. Autophagy proteins are required for secretion in some cases, though the mechanism and cell biological basis for this requirement remain unknown. We found that in colonic goblet cells, proteins involved in initiation and elongation of autophagosomes were required for efficient mucus secretion. The autophagy protein LC3 localized to intracellular multi-vesicular vacuoles that were consistent with a fusion of autophagosomes and endosomes. Using cultured intestinal epithelial cells, we found that NADPH oxidases localized to and enhanced the formation of these LC3-positive vacuoles. Both autophagy proteins and endosome formation were required for maximal production of reactive oxygen species (ROS) derived from NADPH oxidases. Importantly, generation of ROS was critical to control mucin granule accumulation in colonic goblet cells. Thus, autophagy proteins can control secretory function through ROS, which is in part generated by LC3-positive vacuole-associated NADPH oxidases. These findings provide a novel mechanism by which autophagy proteins can control secretion.

*Corresponding author. Department of Pathology and Immunology, Washington University School of Medicine, Box 8118, 660 South Euclid Avenue, St Louis, MO 63110, USA. Tel.: +1 314 362 4214; Fax: +1 314 362 7487; E-mail: stappenb@wustl.edu

Introduction

The inner lining of the colon consists of an expansive single-celled epithelial layer that is coated throughout by a layer of mucus (McGuckin et al, 2011). The epithelium is organized into repeating units, each component consisting of a crypt of Lieberkühn that is surrounded by a 'cuff' of epithelial cells derived from the crypt. A population of epithelial stem cells located at or near the base of each crypt gives rise to multiple lineages, including absorptive colonocytes, hormone-secreting enteroendocrine cells and goblet cells (Snippert et al, 2010). All lineages undergo terminal differentiation as they migrate upwards within the crypt towards the surface cuff (Chang and Leblond, 1971).

Goblet cells are a secretory lineage that specialize in mucus production and begin their differentiation within the crypt. Goblet cells secrete mucus, which forms a layer that overlays the epithelium and forms an important barrier to intestinal microbes (Johansson et al, 2011). Intestinal mucus is composed of multiple highly glycosylated proteins called mucins. In the mouse colon, the major secreted mucins produced by goblet cells are Muc2, Muc5AC and Muc6 (McGuckin et al, 2011). Mucins are stored in secretory granules that are apically localized in the cytoplasm and compartmentalized to this location by a cytoskeletal cage (Specian and Oliver, 1991). Constitutive secretion occurs by fusion of individual mucin granules with the apical plasma membrane (Davis and Dickey, 2008). Mucin granules can accumulate within the goblet cell cytoplasm leading to increased size, which can be secondary to either increased mucin production or diminished secretion (Artis and Grencis, 2008; Zhu et al, 2008).

Loss of autophagy proteins leads to defects in the function of various secretory cell types, though the precise mechanism is unclear (Cadwell et al, 2008; Ebato et al, 2008; Jung et al, 2008; Marino et al, 2010; DeSelm et al, 2011; Ushio et al, 2011). Specifically in the intestine, autophagy proteins are of interest as multiple proteins in this pathway have been identified in genome-wide association studies for inflammatory bowel disease (Franke et al, 2010; Anderson et al, 2011). Autophagy (macroautophagy) is a bulk degradation process in which a curving membrane cistern (a phagophore) encloses cytoplasm into a double membrane-delimited vacuole (an autophagosome). Conversion of the cytosolic protein LC3-I into phosphatidylethanolamine-conjugated LC3-II on the phagophore surface, catalysed by the autophagy proteins Atg7, Atg3 and an Atg12–Atg5 conjugate in association with oligomeric Atg16L1, is essential for phagophore expansion and closure of the autophagosome. Autophagosomes subsequently fuse with endosomes to form

an amphisome that in turn fuses with lysosomes for degradation of cytoplasmic components (Levine *et al*, 2011).

The functional importance of this convergence between autophagic and endocytic pathways has been shown during bacterial infections (Seglen, 2008). For example, bacteria-containing phagosomes must be targeted to the autophagic pathway for their maturation and delivery to the lysosome in a process termed as LC3-associated phagocytosis or LAP (Sanjuan *et al*, 2007; Florey *et al*, 2011; Henault *et al*, 2012). Furthermore, NADPH oxidase-derived reactive oxygen species (ROS) are essential for the interaction of phagocytosis and autophagy pathways (Huang *et al*, 2009). The NADPH oxidase family consists of several cytochrome subunits (Nox1–5), and additional cytosolic regulatory proteins including a common membrane bound subunit p22phox, which is important for the stabilization of the oxidase. The different isoforms of cytochrome subunits are differentially expressed depending on the cell type. Importantly, expression of these isoforms is not limited to phagocytic cells where NADPH oxidase-derived ROS function in bactericidal roles. These oxidases are also expressed in various epithelial cell types including the intestine; however, their functional significance in these cell types is unclear (Bedard and Krause, 2007).

We evaluated the function of autophagy proteins in the colonic epithelium of mice and found mucin accumulation in goblet cells lacking autophagy proteins. The mechanistic basis of a requirement for autophagy proteins in secretory epithelial cells is not well understood. This is in part due to the fact that the precise cellular location of autophagosomes in tissues visualized by endogeneous LC3 has been challenging. Here, we performed studies using loss-of-function mutations for autophagy proteins, endogenous LC3β localization and a novel epithelial cell-culture system. We found that LC3 localized to complex multi-vesicular structures that were also positive for endosomal markers and NADPH oxidases in goblet cells. Loss of autophagy proteins, endocytosis and NADPH oxidase components all resulted in diminished ROS generation as well as accumulation of mucin within goblet cells. Importantly, these defects in mucin accumulation resulting from the loss of function of autophagy, endocytosis and NADPH oxidase function could all be rescued by exogenous ROS, suggesting functional linkages between these processes.

Results

Autophagy proteins control mucin granule accumulation in colonic goblet cells in vivo

To assess the role of the autophagy protein Atg5 in the colonic epithelium, we compared Alcian blue-stained sections from mice lacking Atg5 expression in the intestinal epithelium (*Atg5^{f/f}*, Hara *et al*, 2006; Villin-Cre +, Madison *et al*, 2002 or *Atg5VC*) to littermate controls (*Atg5^{f/f}*; Villin-Cre − as well as *Atg5^{f/+}*; Villin-Cre +). In the intestine, Alcian blue labels highly glycosylated proteins most notably goblet cell mucins. This staining showed that *Atg5VC* mice contained larger areas of cytoplasmic mucin within goblet cells as compared to controls (Figure 1A). We confirmed this finding using immunostains for Muc2, an abundant mucin produced by colonic goblet cells, as well as the lectin *Ulex europaeus* agglutinin 1 (UEA, Supplementary Figure S1A and B),

which labels L-fucose groups found on both intracellular mucin and secreted mucus (Falk *et al*, 1994). This enlarged goblet cell phenotype in *Atg5VC* mice was apparent in immature goblet cells located in the crypt base as well as in mature goblet cells in the upper portion of crypts. We used these histological sections to quantify the area of mucin staining per goblet cell in the upper crypt region and confirmed that *Atg5VC* colonic goblet cells contained an enlarged area of Alcian blue-positive staining as compared to littermate controls (Figure 1B). Importantly, *Atg5VC* mice contained similar numbers of goblet cells per crypt as compared to controls (Figure 1C). Comparison of haematoxylin and eosin-stained sections showed no obvious defects in colonic crypt height, epithelial proliferation and cell death indicating no obvious change in epithelial turnover (Supplementary Figure S1C–F). Additionally, there was no change in the presence of inflammatory cells in colons of *Atg5VC* mice (Supplementary Figure S1G). Therefore, our interpretation is that colonic goblet cells in *Atg5VC* mice contained normal numbers of goblet cells that showed abnormal mucin accumulation.

We previously showed that autophagy gene-deficient Paneth cells contain abnormal secretory granules (Cadwell *et al*, 2008). However, transmission electron microscopic analysis of colonic goblet cells from *Atg5VC* and control mice showed no obvious differences in the size and the shape of individual mucin granules (Figure 1D), indicating that the role of autophagy proteins differs in these two secretory cell types. Furthermore, the density of mucin granules within goblet cells was similar in *Atg5VC* and control mice (Figure 1E). We did observe that *Atg5VC* goblet cells contained a significantly greater number of mucin granules than controls (Figure 1F). Thus, the major defect in Atg5-deficient colonic goblet cells was an accumulation of ultrastructurally normal-appearing mucin granules.

The accumulated mucin granules in *Atg5VC* colonic goblet cells suggested a defect in granule exocytosis. Therefore, we analysed mucosal surfaces for mucus extravasation from crypt openings of *Atg5VC* and control mice. To visualize mucus emerging from crypts in whole-mount preparations, we used fluorescently conjugated-UEA (Figure 1G) as well as scanning electron microscopic analysis of the mucosal surface (Figure 1H). Using both methods, we observed regions of diminished mucus emerging from colonic crypts of *Atg5VC* mice compared to controls. These findings supported our hypothesis that *Atg5VC* goblet cells had a defect in granule exocytosis.

We next tested the function of additional autophagy proteins in colonic goblet cells. We analysed colons from *Atg7^{f/f}*; Villin-Cre + (Komatsu *et al*, 2005) and *LC3β^{−/−}* (Cann *et al*, 2008) mice and found that loss of function of either of these genes also led to mucin accumulation in colonic goblet cells (Supplementary Figure S2A–D). Taken together, these data showed that the autophagy proteins Atg5, Atg7 and LC3β played a common role in regulating goblet cell mucin accumulation.

Atg5 controls mucin granule accumulation in cultured colonic goblet cells

As a tool to further dissect the mechanisms and the involvement of additional autophagy genes involved in mucin granule accumulation in Atg5-deficient cells, we established
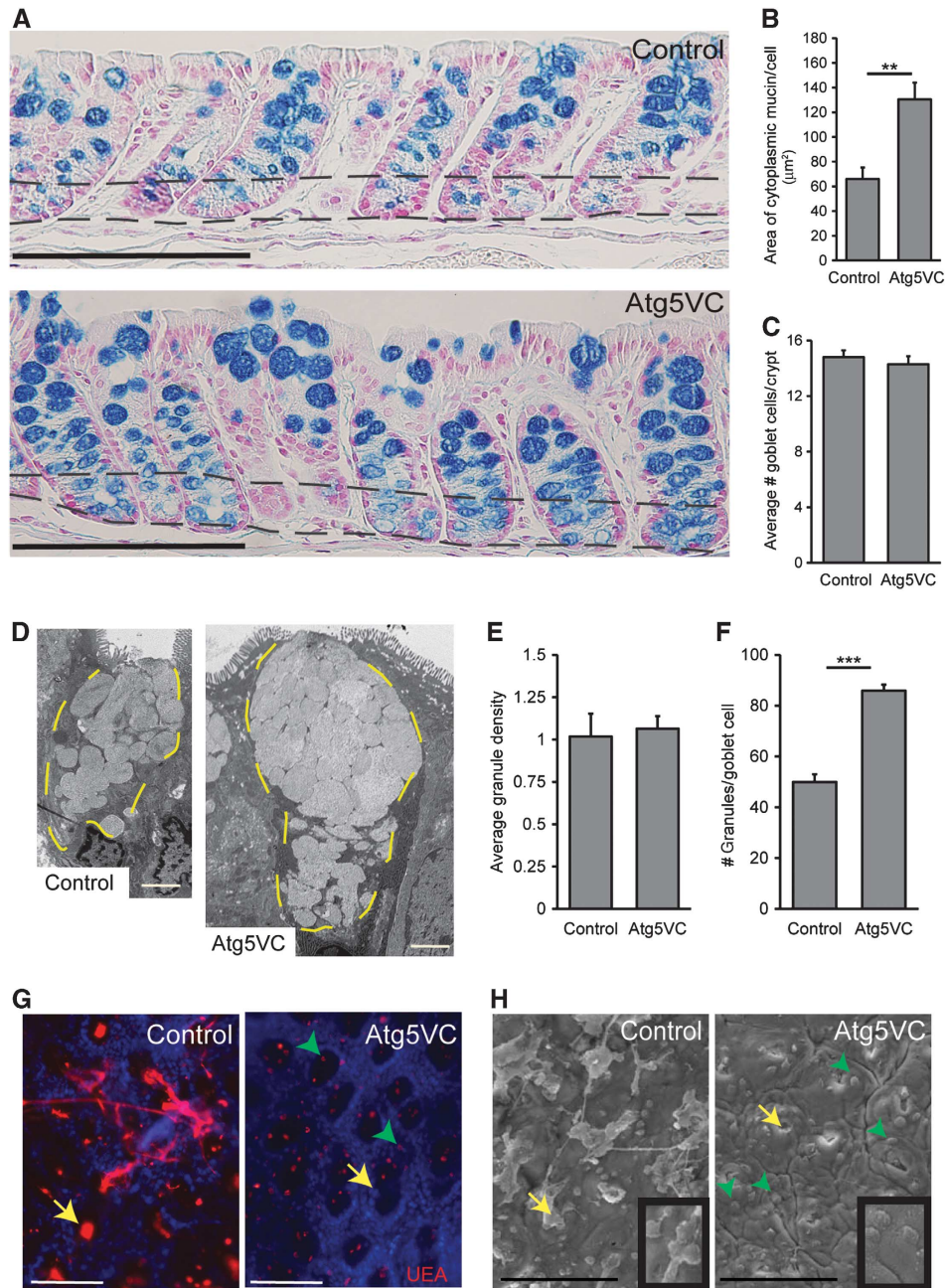
Figure 1 Atg5-deficient goblet cells accumulate mucin. (**A**) Alcian blue-stained sections of descending colons from control and *Atg5VC* mice. The area between the two black dashed lines indicates the crypt base where epithelial progenitors and nascent goblet cells reside. Bars = 200 μm. (**B**) Quantification of average mucin area/goblet cell in control and *Atg5VC* mice ($n = 5$–7 mice/group from 3 independent experiments; 100 goblet cells measured/mouse). **$P < 0.01$ as determined by the Student's *t*-test. This analysis was performed on upper crypt goblet cells (above the upper dashed line in **A**). (**C**) Quantification of the average number of goblet cells per crypt ($n = 3$ mice/group; over 100 crypts measured/mouse). (**D**) TEM images of upper crypt goblet cells from control and *Atg5VC* transverse colons. The yellow dashed lines outline the mucin granules in the apex of the cells. Bars = 2 μm. (**E**, **F**) Quantification of (**E**) the average granule density and (**F**) the average number of mucin granules/goblet cell ($n = 3$ mice/group and 20 goblet cells evaluated/mouse). ***$P < 0.001$ as determined by the Student's *t*-test. (**G**, **H**) Whole-mount images of the mucosal surface from control and *Atg5VC* transverse colons. Whole-mount colonic samples were either stained with *Ulex europaeus* agglutinin-1 (UEA) that labelled mucus (**G**) or analysed by the scanning electron microscopy (**H**). Yellow arrows indicate the crypt opening orifices. Green arrowheads indicate goblet cells protruding from the surface epithelium of *Atg5VC* mice (insets in **H** show higher power image of the latter). Bars = 100 μm.

an *in vitro* system for colonic epithelial cells that contained goblet cells. We modified a colonic epithelial spheroid culture system (Figure 2A) that is enriched in stem cells (Miyoshi *et al*, 2012). To promote goblet cell differentiation, we reduced Wnt ligands and added DAPT, an inhibitor of Notch signalling to the culture media (Pellegrinet *et al*,

2011; Supplementary Figure S3A). We also added LPS to induce mucin expression. This treatment increased the number of Muc2-positive goblet cells (Figure 2B). qRT-PCR for Muc2 and Atoh1 additionally confirmed the enhanced commitment to goblet cell differentiation in DAPT-treated colonic epithelial cultures (Figure 2C and D). Herein, all *in vitro*

experiments with colonic epithelial cells were conducted using these conditions.

Using this system to culture and differentiate colonic epithelial cells, we tested the role of Atg5 in goblet cells. We found that goblet cells generated from *Atg5VC* colonic epithelial stem cells showed greater mucin accumulation compared to controls as evidenced by an increased area of cytoplasmic Muc2 as well as UEA staining (Figure 2E–G). Importantly, there was no difference in Muc2 mRNA levels in *Atg5VC* epithelial cultures compared to controls (Figure 2H). Collectively, these results demonstrated that the loss of Atg5 *in vitro* recapitulated the goblet cells defects observed in *Atg5VC* mice.

We then used our *in vitro* system to test the role of additional autophagy proteins in goblet cell function. In particular, we wanted to distinguish between conventional autophagy or related processes such as LAP (Florey *et al*, 2011; Henault *et al*, 2012). Specifically, we evaluated the role of Atg14, which is a required component of the class II Pi3K complex that initiates autophagy. We also evaluated FIP200, which is also required for autophagy initiation but is not required for LAP ((Florey *et al*, 2011; Martinez *et al*, 2011). To study the role of these upstream autophagy genes, we isolated colonic epithelial spheroids from *FIP200*$^{f/f}$ and *Atg14*$^{f/f}$ mice and delivered recombinant Tat-Cre recombinase (Morimoto *et al*, 2010). This transient delivery of Cre efficiently mediates recombination of floxed alleles (Shaw *et al*, 2008; Morimoto *et al*, 2010). We tested three clones that contained fully excised floxed alleles (Supplementary Figure S3B and C) for goblet cell mucin accumulation. All lines from *FIP200*$^{f/f}$ + Tat-Cre and *Atg14*$^{f/f}$ + Tat-Cre colonic epithelial spheroids showed increased mucin accumulation compared to controls (Figure 2I–K). This was similar to what we observed with *Atg5VC* epithelial cultures. These results demonstrated that factors involved in the initiation and maturation of autophagosomes, including one protein, FIP200, that is not required for LAP were required for colonic goblet cell function.

Intersection of autophagy proteins and endocytosis in colonic goblet cells

We next analysed intestinal tissue sections of wild-type mice stained for endogeneous LC3β to localize autophagosomes. Targeting of LC3β to autophagosomes requires Atg5 (Levine *et al*, 2011); therefore, we also analysed tissue sections from *Atg5VC* mice. We detected LC3β in concentrated cytoplasmic regions of colonic crypt epithelial cells from control but not *Atg5VC* mice (Figure 3A). By this analysis, LC3β signal did not appear to be associated with the mucin granule compartment of goblet cells.

To determine the subcellular membrane localization of LC3β in crypt epithelial cells, we performed immunogold transmission electron microscopy. In control, but not in *Atg5VC* mice, we detected LC3β-positive membranes within the goblet cell cytoplasm (Figure 3B, inset). Interestingly, many of these LC3β-positive membranes were multi-vesicular vacuoles that were morphologically quite distinct from conventional autophagosomes, which are characterized by multiple or double delimiting membranes. We detected no LC3β signal on mucin granules or plasma membranes (Supplementary Figure S4).

To better understand the pathways that were altered in response to the loss of Atg5 expression, we performed microarray analysis of mRNAs isolated from laser capture microdissected colonic epithelial cells. We compared gene expression in crypt base cells from *Atg5VC* versus control mice, as this area of the epithelium is enriched for immature goblet cells (Chang and Leblond, 1971) and thus would allow for analysis of the earliest changes associated with loss of *Atg5*. Such analysis can elucidate pathways and compensatory changes that occur in response to loss of function of a specific gene.

We then used the bioinformatics suite, DAVID (Huang da *et al*, 2009a, 2009b) to derive enriched KEGG pathways and Gene Ontology terms from the list of 320 transcripts that were significantly altered in the *Atg5*-deficient epithelium. The most significantly altered pathway determined by KEGG pathway analysis was endocytosis (Figure 3C; Supplementary Figure S5A and B). Significantly enriched GO terms for the domain 'cellular components' included endosome as well as other endomembrane compartments (Supplementary Figure S5C). These results were interesting since recent studies have shown endosomes and the plasma membrane can serve as potential membrane sources for autophagosomes (Ravikumar *et al*, 2010; Longatti *et al,* 2012). Additionally, intersection of autophagic with endocytic vesicles has been well documented (Seglen, 2008; Razi *et al*, 2009). Importantly, we found no significant differences between *Atg5VC* and control samples when comparing mRNAs encoding secreted mucins suggesting that there is no obvious defect in mucin production (Supplementary Figure S5C).
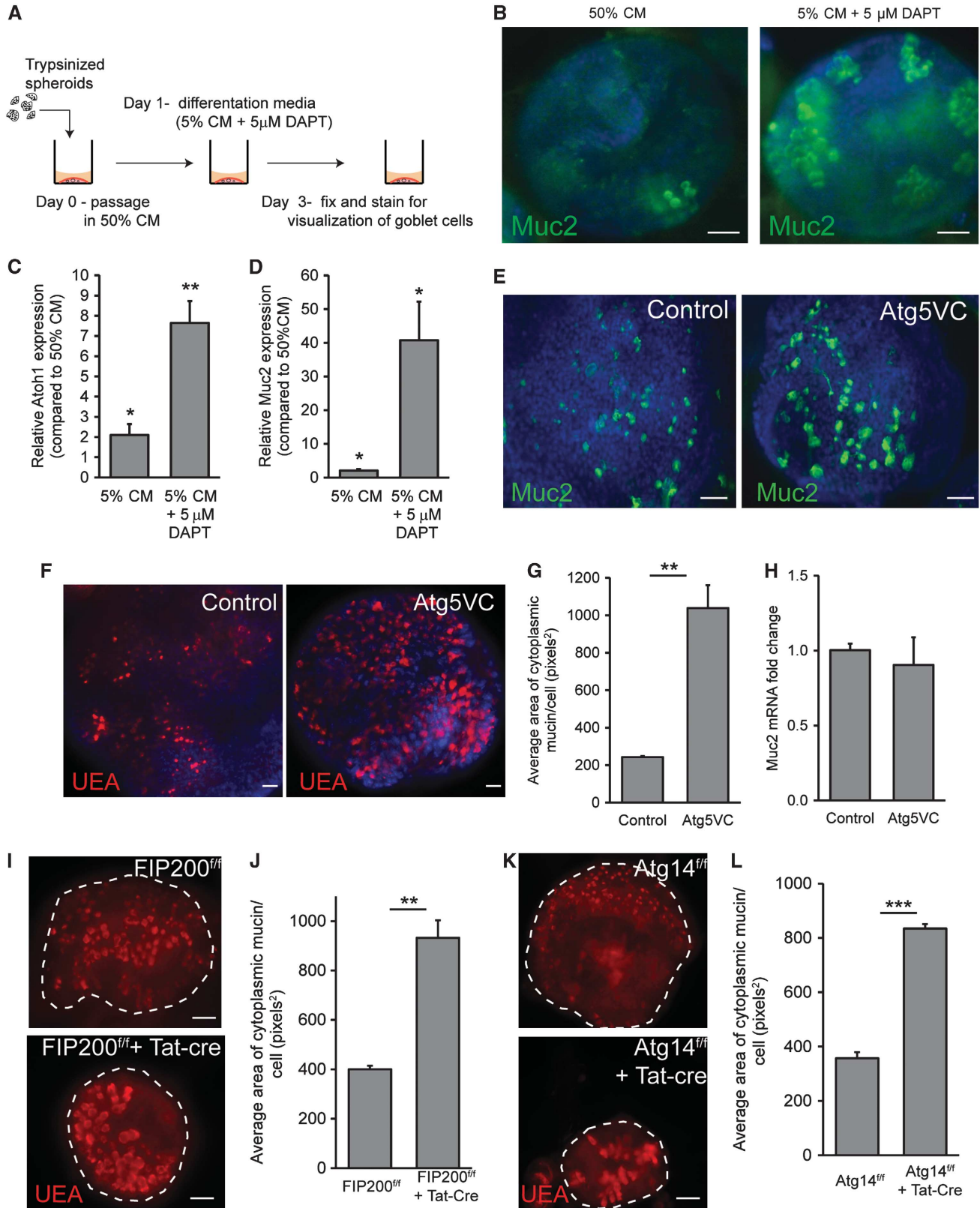
Endocytosis plays a role in mucin granule accumulation

To investigate the possibility that endosomes intersect with the autophagic pathway, we performed double label immunogold transmission electron microscopic studies, and found that LC3β-positive vacuoles in goblet cells were also positive for the early endosomal marker EEA1 (Figure 3D). Additionally, we found that these LC3β-positive vacuoles also co-labelled with markers of late endosomes (Rab7) and lysosomes (Lamp1), indicating that LC3β can be present on organelles throughout endocytic maturation process. However, we did not detect co-labelling of LC3β and Rab11 indicating that LC3β was not present on recycling endosomes (Figure 3E–G).

We next determined whether EEA1 and LC3β co-localize in colonic epithelial cells grown in monolayers (Figure 4A). In wild-type colonic epithelial cells, we observed intracellular LC3β puncta. Interestingly, we found a significant co-localization of endogeneous LC3β and EEA1 (Figure 4B), consistent with the presence of the double positive vacuoles observed *in vivo* by immunogold localization. Treatment with Dynasore, an inhibitor of dynamin-mediated endocytosis, did not significantly reduce the number of LC3β puncta, but did diminish co-localization of LC3β with EEA1 (Figure 4C and D). Additionally, LC3 II conversion was unchanged in Dynasore-treated spheroids compared to controls. Also, autophagic flux was not altered by Dynasore treatment as determined by LC3 II conversion using the lysosomal inhibitor bafilomycin A1 (bafA1; Figure 4E). These results demonstrated that inhibition of endocytosis did not affect autophagy.

We next tested the role of endocytosis in mucin granule accumulation. Importantly, cultured wild-type colonic spheroids treated with Dynasore resulted in mucin accumulation in goblet cells (Figure 4F and G) similar to what was observed in the absence of autophagy proteins. Additionally, treatment of colonic spheroids with Pitstop 2, an inhibitor of clathrin-mediated endocytosis, resulted in a similar increase in mucin accumulation as compared to colonic spheroids treated with a highly related molecule that binds clathrin but does not inhibit endocytosis (negative control for Pitstop 2;
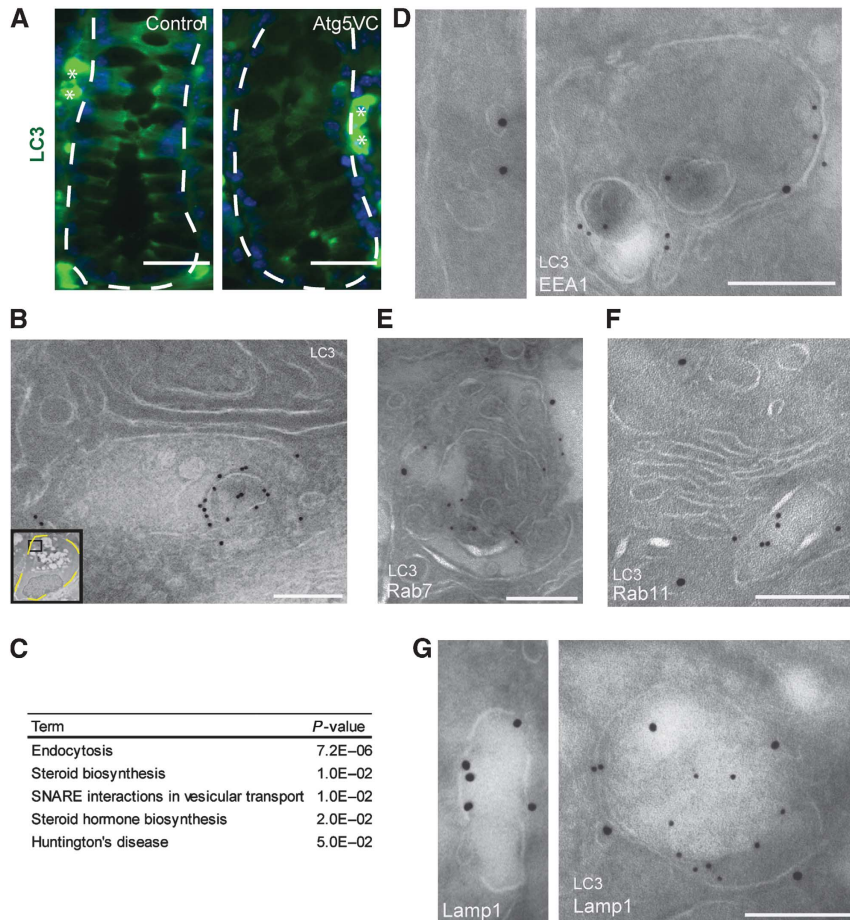
Supplementary Figure S6). These experiments showed that clathrin-mediated endocytosis played a role in mucin granule accumulation.

### NADPH oxidases contribute to LC3 and EEA1 co-localization and mucin accumulation

On the basis of prior studies, NADPH oxidases are a potential link between autophagosomes and endosomes (Sanjuan *et al*, 2007; Huang *et al*, 2009). NADPH oxidases are known to localize to endosomes in macrophages and neutrophils (Casbon *et al*, 2009; Lamb *et al*, 2012) and are required for the recruitment of LC3β to bacteria-containing phagosomes (Huang *et al*, 2009). On the basis of these findings, we hypothesized that NADPH oxidases are a functional link between the autophagic and endocytic pathways in goblet cells. First, we determined whether loss of NADPH oxidase function resulted in diminished co-localization of LC3 and EEA1. p22phox is a common membrane component of most

Term	P-value
Endocytosis	7.2E−06
Steroid biosynthesis	1.0E−02
SNARE interactions in vesicular transport	1.0E−02
Steroid hormone biosynthesis	2.0E−02
Huntington's disease	5.0E−02

Figure 3 LC3β is localized to EEA1-positive multi-vesicular vacuoles within colonic goblet cells. (**A**) Images of colonic sections stained for LC3β (green) from control and *Atg5VC* mice. The white-dashed lines indicate the border between the basal surface of the crypt epithelium and the mesenchyme. White asterisks denote non-specific plasma cell staining from the mouse monoclonal anti-LC3β antibody. Bars = 50 μm. (**B**) Immunogold transmission electron microscopic image for LC3β in a colonic goblet cell from a wild-type mouse. The inset is a low power image of the entire goblet cell. The black box within the inset indicates the area shown in this panel. Note this area is not associated with mucin granules. Bar = 500 nm. (**C**) Enriched KEGG pathways for Atg5-deficient epithelial cells obtained from a microarray comparing control and *Atg5VC* colonic crypt base epithelium. *P*-values were determined by modified Fisher's exact test. (**D–G**) Double label immunogold transmission electron microscopic images from wild-type mice for LC3β (12 nm particles) and EEA1 (**D**), Rab7 (**E**), Rab11 (**F**), or Lamp1 (**G**) (18 nm particles). Bars = 200 nm.

Figure 2 Atg5-deficient colonic epithelial spheroids accumulate cytoplasmic mucin within goblet cells. (**A**) Schematic for the generation of differentiated goblet cells within colonic epithelial spheroid cultures. (**B**) Representative whole-mount images of single spheroids cultured in either 50% conditioned media (CM) or 5% CM + 5 μM DAPT and stained for Muc2 (green) to visualize goblet cells. Bars = 20 μm. (**C, D**) Graph of relative expression (as measured by qRT-PCR) of Atoh1 (**C**) and Muc2 (**D**) mRNAs comparing spheroids grown in either 5% CM or 5% CM + DAPT to spheroids grown in 50% CM (*n* = 4–5 samples/group). Error bars indicate s.e.m. *$P < 0.05$; **$P < 0.01$ as determined by a two-tailed Student's *t*-test. (**E, F**) Images of colonic epithelial spheroids isolated from control and *Atg5VC* mice grown in 5% CM + DAPT and stained for Muc2 (green: **E**) or with the lectin, UEA (red: **F**). Bars = 20 μm. (**G**) Quantification of average mucin area/goblet cell. Error bars indicate s.e.m. (*n* = 6 samples/group; 100 cells were quantified/sample; **$P < 0.01$ as determined by a two-tailed Student's *t*-test). (**H**) Relative expression of Muc2 mRNA in differentiated spheroids from control and *Atg5VC* mice as measured by qRT–PCR (*n* = 4–5 samples/group). No statistically significant differences were found in Muc2 expression as determined by the Student's *t*-test. (**I, K**) Images of *FIP200^{f/f}* (**I**) and *Atg14^{f/f}* (**K**) colonic epithelial spheroids treated with recombinant Tat-Cre and stained with UEA (red). (**J, L**) Quantification of average mucin area/goblet cell. Error bars indicate s.e.m. (*n* = 6 samples/group; 100 cells were quantified/sample; **$P < 0.01$ and ***$P < 0.001$ as determined by a two-tailed Student's *t*-test).
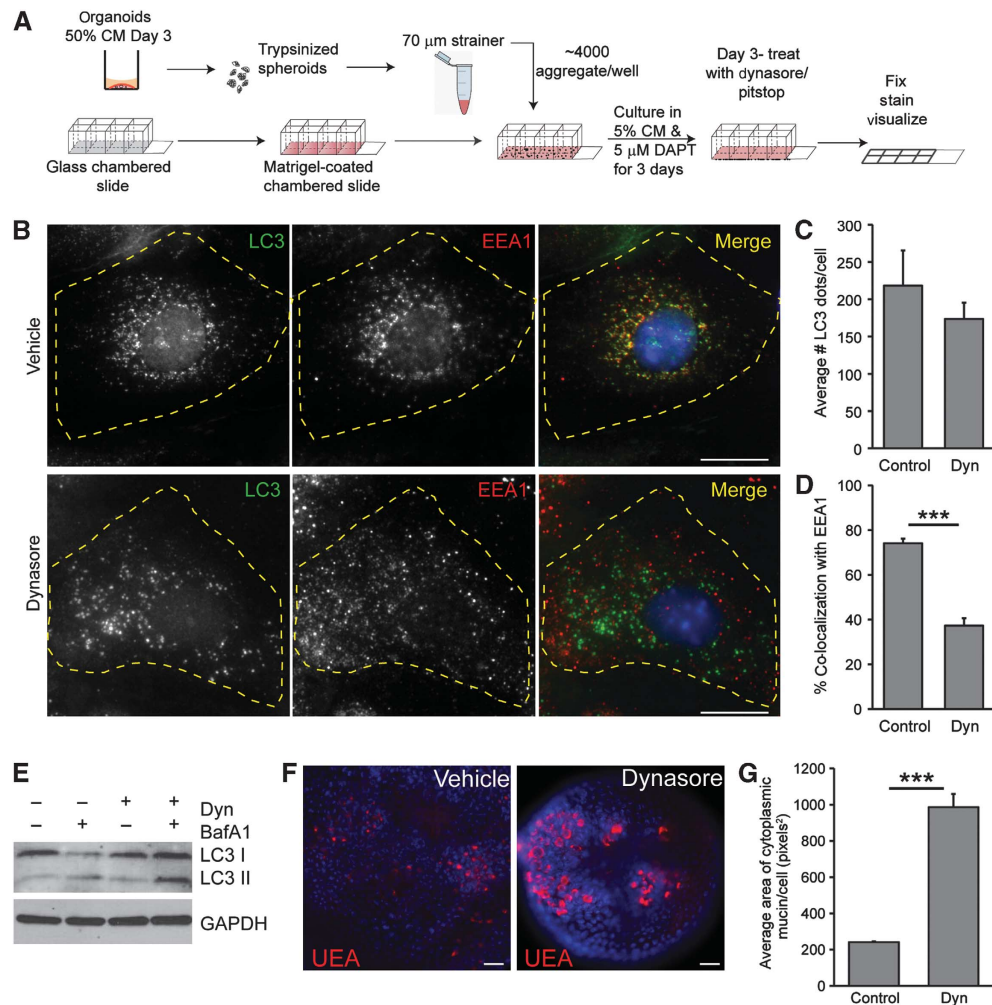
Figure 4 Inhibition of endocytosis results in goblet cell mucin accumulation. (**A**) Schematic for the generation of differentiated colonic epithelial cells grown in a monolayer. (**B**) Colonic epithelial monolayers from wild-type mice treated with either vehicle or 100 μM Dynasore and stained for LC3β (green) and EEA1 (red). Bars = 5 μm. (**C, D**) Quantification of average number of LC3β dots per cell (**C**) and the percentage of LC3β dots that co-localized with EEA1 per cell (**D**) ($n = 3$ experiments/group; 25–30 cells/experiment). (**E**) LC3 immunoblots of epithelial spheroids treated with 100 μM Dynasore and 100 nM BafA1 as indicated. GAPDH is a loading control. Representative image is shown from $n = 3$ experiments. (**F**) Images of wild-type colonic epithelial spheroids labelled with TRITC-UEA (red) after treatment with either vehicle or 100 μM Dynasore. Bars = 20 μm. (**G**) Quantification of average mucin area/goblet cell ($n = 6$ samples/group; 150 cells were quantified/sample). Error bars indicate s.e.m. ***$P < 0.001$ as determined by the Student's *t*-test.

NADPH oxidases. Using colonic spheroids developed from *p22phox* mutant mice (*Cyba^{nmf333/nmf333}*, herein referred to as *p22 mut*), we found that p22phox was required for maximal co-localization of LC3β and EEA1 in epithelial cells (Figure 5A–C). However, the absence of p22phox did not alter LC3 II conversion or autophagic flux (Figure 5D). Additionally, p22phox did not appear to accumulate in the presence of the lysosomal inhibitor, bafA1 suggesting that p22phox is not degraded by autophagy (Supplementary Figure S7A). Collectively, these results supported a role for NADPH oxidases in the intersection of autophagy and endocytosis.

Next, we determined the localization of p22phox in colonic epithelial cells. By double-label immunogold electron microscopy, we found that p22phox localized to LC3β-negative small vacuoles, which co-labelled with the endosomal marker Rab5 as well as LC3β-positive multi-vesicular vacuoles (Figure 5E; Supplementary Figure S7B). We confirmed this finding *in vitro* and found that a subset of LC3β co-localized

with p22phox in colonic epithelial cells by double label immunofluorescence analysis (Figure 5F). The percent co-localization was similar to the percent co-localization of LC3 and EEA1 (Figure 5C).

To determine whether the requirement of NADPH oxidases influenced intracellular mucin accumulation in goblet cells, we next stained colonic spheroids from *p22 mut* and control mice for UEA. We found greater mucin accumulation in the *p22 mut* goblet cells as compared to controls (Figure 5G and H). This finding was similar to what we observed either when Atg5 was deleted or when endocytosis was blocked. To test whether other components of the NADPH oxidase complex were also important for this process, we examined the goblet cells in mice deficient for p47phox, a cytosolic subunit of the Nox2 NADPH oxidase and found enhanced mucin accumulation in colonic goblet cells of *p47phox^{−/−}* mice as compared to controls (Supplementary Figure S7C–E). Together, these data indicate a new role for NADPH oxidases in the function of goblet cells.
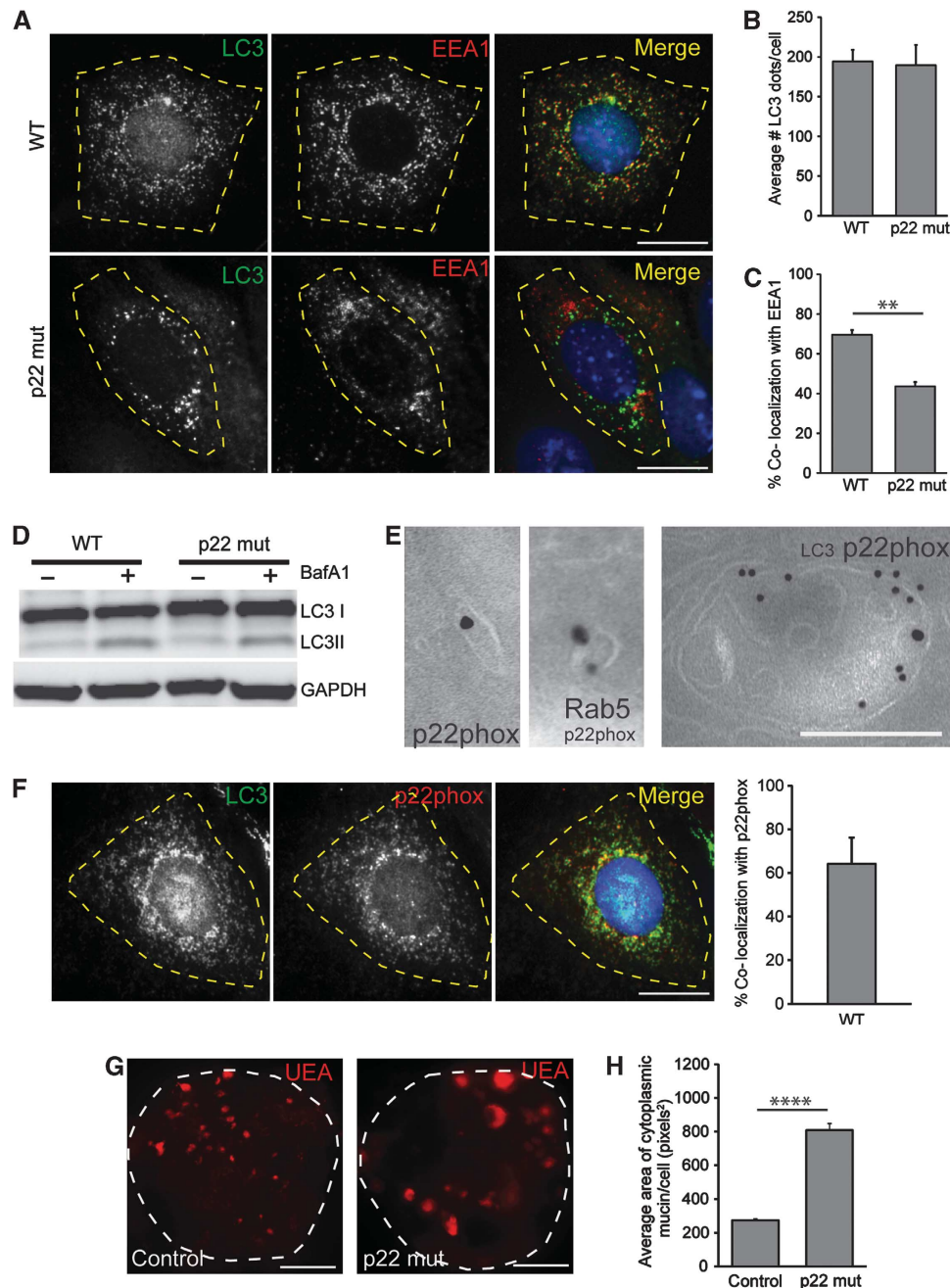
Figure 5 NADPH oxidases are required for endosome/autophagosome co-localization and control mucin granule accumulation. (**A**) Colonic epithelial monolayers from a wild-type and *p22 mut* mouse stained with LC3β (green) and EEA1 (red). Bar = 5 μm. (**B, C**) Quantification of average number of LC3β dots per cell (**B**) and the percentage of LC3β dots that co-localized with EEA1 per cell (**C**) (*n* = 3 experiments/group; 25–30 cells/experiment). (**D**) LC3 immunoblots of either wild-type or p22 mut epithelial spheroids treated with 100 nM BafA1 as indicated. Representative image is shown from *n* = 3 experiments. (**E**) Double label immunogold transmission electron microscopic images for LC3β (12 nm particles) and p22phox (18 nm particles) showing a p22phox-positive single membrane cytoplasmic vesicle (**D**) and a p22phox-, LC3β-positive vacuole (**E**). Bars = 200 nm. (**F**) Colonic epithelial monolayers from a wild-type mouse stained for LC3β (green) and p22phox (red) and quantification of percent LC3β dots co-localized with p22phox per cell, Bar = 5 μm. (**G**) Colonic epithelial cell spheroids from control and *p22 mut* mice stained with TRITC-UEA to label goblet cell mucin. Bars = 50 μm. (**H**) Quantification of average mucin area/goblet cell (*n* = 6 samples/group; 150 cells were quantified/sample). Error bars indicate s.e.m. **P < 0.01; ****P < 0.0001 as determined by the Student's *t*-test.

Endocytosis and Atg5 are required to generate maximal ROS in colonic epithelial cells

Since NADPH oxidases were required for mucin secretion, we considered the possibility that products of this enzyme complex, ROS, may be the molecules responsible for functionally linking NADPH oxidase and mucin granule accumulation. We found that wild-type spheroids produced significantly higher levels of ROS as compared with *p22 mut* spheroids or wild-type spheroids treated with diphenyleneiodonium (DPI) chloride, an inhibitor of NADPH oxidases. Importantly, we found that Atg5-deficient spheroids or wild-type spheroids treated with Dynasore exhibited significantly diminished ROS
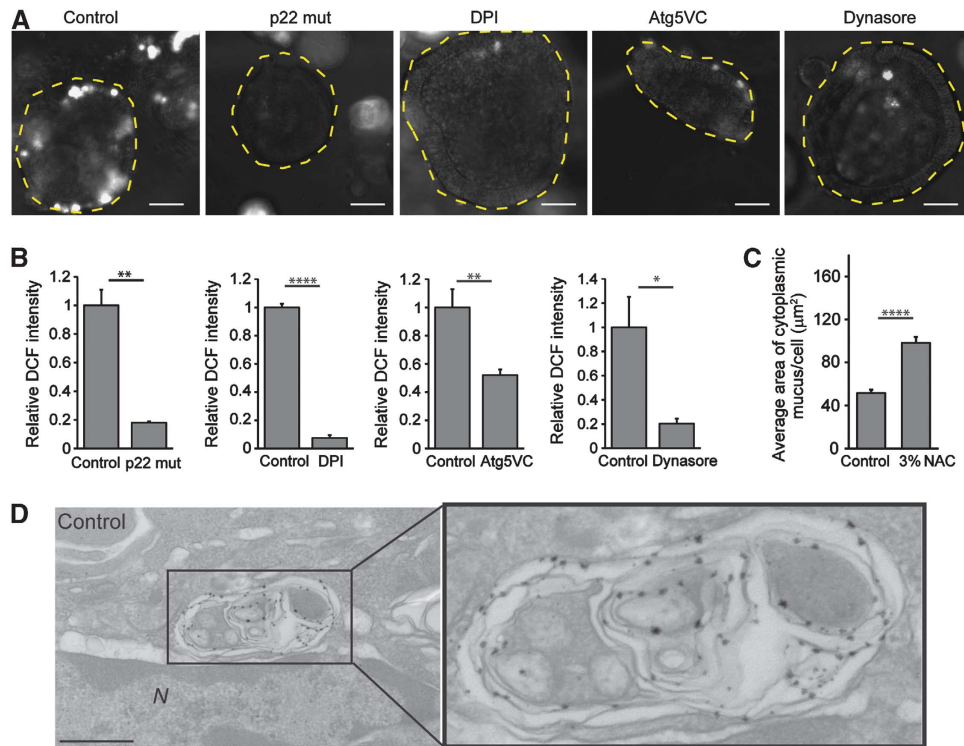
Figure 6 Goblet cell mucin accumulation correlates with diminished ROS production. (**A**) Colonic epithelial cell spheroids from $p22phox^{-/-}$, *Atg5VC* and wild-type mice. Wild-type spheroids were treated with vehicle (control), 10 μM DPI (NADPH oxidase inhibitor) or 100 μM Dynasore. Intracellular ROS in live cells were labelled by 5 μM DCF. Bars = 100 μm. (**B**) Quantification of fluorescent DCF normalized to control ($n = 3$ independent experiments/group; 30 spheroids quantified/experiment). (**C**) Quantification of average area of cytoplasmic mucin from wild-type mice treated with 3% NAC as compared to controls ($n = 6$–7 mice/group). Error bars indicate s.e.m. *$P < 0.05$; **$P < 0.01$; ****$P < 0.0001$ as determined by the Student's *t*-test. (**D**) TEM images of colonic epithelial monolayers treated with cerium chloride. The presence of electron dense precipitate is indicative of ROS production. Bar = 500 nm.

production as compared to controls (Figure 6A and B). These results indicated that both endosomes and autophagy proteins were required for efficient ROS production, and that the major source of ROS was NADPH oxidases. The lack of ROS generation in *p22 mut*, Atg5-deficient and Dynasore-treated spheroids correlated with enhanced mucin accumulation. We tested the requirement for ROS production *in vivo* by treating wild-type mice with the ROS scavenger *N*-acetylcysteine (NAC). We found enhanced mucin accumulation in colonic goblet cells of NAC-treated mice as compared to controls (Figure 6C; Supplementary Figure S8). In order to localize ROS production within wild-type colonic epithelial cells to subcellular structures, we treated colonic epithelial monolayers with cerium chloride (Vazquez-Torres *et al*, 2000; Lam *et al*, 2011). Using this method, an electron dense precipitate detected by transmission electron microscopy indicates areas of ROS production. We found that complex multi-vesicular vacuoles contained precipitate in wild-type cells (Figure 6D). Collectively, these results supported the hypothesis that localized NADPH oxidase-dependent ROS production played an important functional role in mucin accumulation.

Exogeneous ROS restore defects in goblet cell mucin accumulation

We next tested whether administration of exogenous ROS could restore the defect in mucin accumulation observed in the absence of Atg5, endocytosis or functional NADPH oxidases. Therefore, we added hydrogen peroxide to Atg5-defi-

cient intestinal epithelial spheroid cultures. This resulted in increased intracellular ROS within spheroid cultures as measured by DCF fluorescence (Figure 7A). We found that hydrogen peroxide treatment led to diminished intracellular mucin in Atg5-deficient goblet cells as compared to vehicle-treated controls (Figure 7B and C). These changes in intracellular mucin content were likely not a result of altered mucin production as Muc2 mRNA levels were not significantly different across all groups (Figure 7D). Additionally, treatment of hydrogen peroxide did not alter autophagic flux (Supplementary Figure S9A). We also found that administration of hydrogen peroxide to Dynasore-treated spheroids as well as *p22 mut* spheroids resulted in diminished intracellular mucin compared to vehicle-treated controls (Figure 7E–H).

Intracellular ROS generation can lead to elevated cytosolic calcium (Wang *et al*, 1999; Cheranov and Jaggar, 2006; Granados *et al*, 2006; Hidalgo *et al*, 2006; Bedard and Krause, 2007). In turn, elevated cytosolic calcium levels can lead to mucin granule release (Abdullah *et al*, 1997; Conway *et al*, 2003; Davis and Dickey, 2008). Therefore, we explored whether calcium mediated the effect of ROS on mucin granule accumulation in colonic goblet cells. Using Fluo-4 to measure intracellular calcium levels, we found that *Atg5VC* and *p22 mut* spheroids contained diminished calcium levels relative to wild-type spheroids (Supplementary Figure S9B). The addition of a cell permeable calcium chelator, BAPTA-AM, inhibited the effect of hydrogen peroxide on mucin release in both Atg5-deficient and *p22 mut* spheroids (Figure 7I).
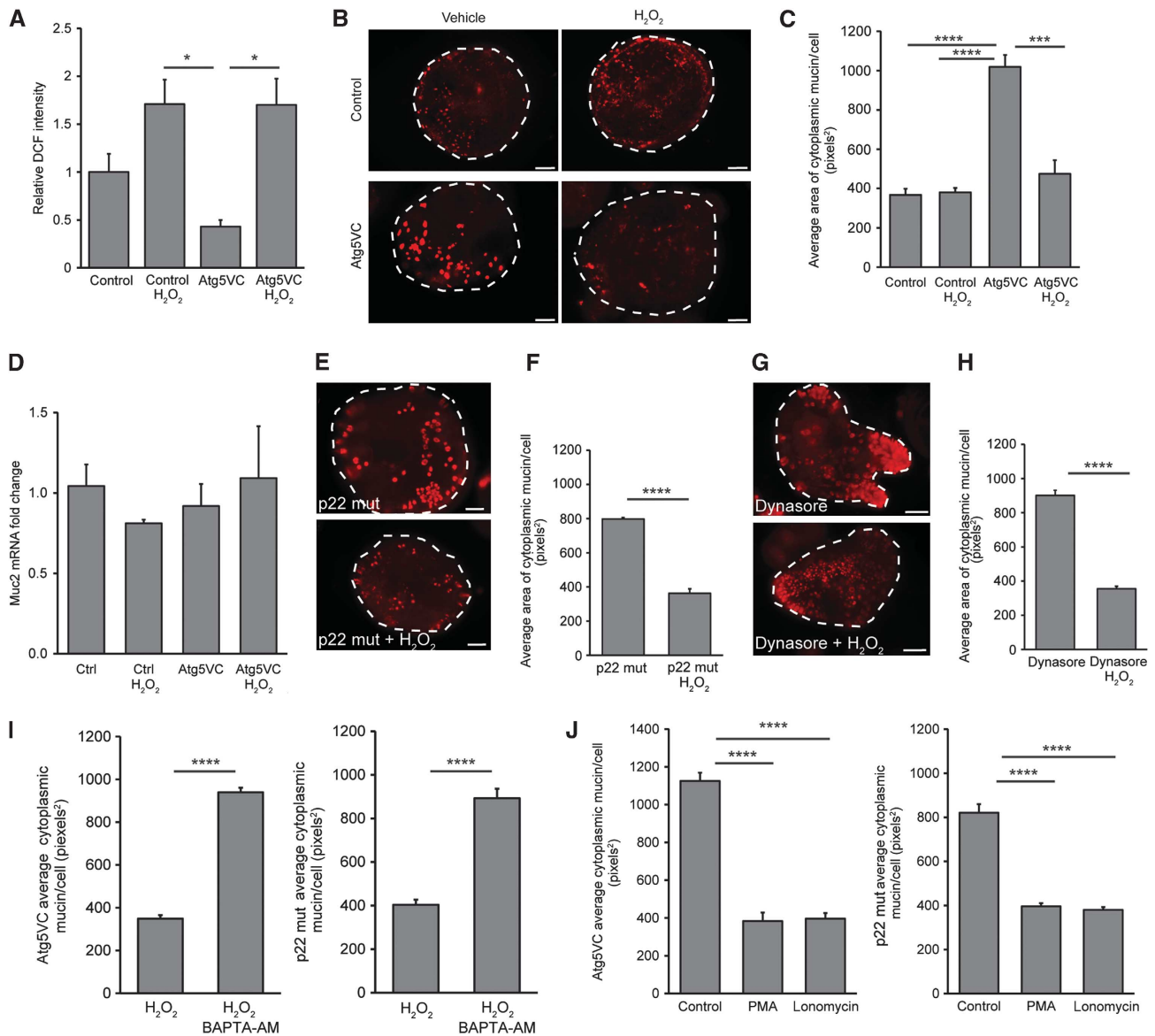
Figure 7 Exogenous ROS can restore mucin granule accumulation defects. (**A**) Quantification of fluorescent DCF normalized to controls ($n = 3$ independent experiments/group; 10–30 spheroids quantified/culture). *$P < 0.05$ as determined by ANOVA with Tukey's multiple post-test comparisons. (**B**) Images of control and *Atg5VC* colonic epithelial spheroids labelled with TRITC-UEA (red) after treatment with either vehicle or 300 μM H_2O_2. Bars = 20 μm. (**C**) Quantification of average mucin area/goblet cell ($n = 6$ samples/group; 150 cells were quantified/sample). ***$P < 0.001$, ****$P < .0001$ as determined by ANOVA with Tukey's multiple post-test comparisons. (**D**) Relative expression of Muc2 mRNA in differentiated spheroids from control and *Atg5VC* mice treated with either vehicle or 300 μM H_2O_2 as measured by qRT–PCR. No statistically significant differences were found in either group as determined by ANOVA. (**E, G**) Images of *p22 mut* or Dynasore-treated colonic epithelial spheroids (mucin is labelled with TRITC-UEA; red) after treatment with either vehicle or 300 μM H_2O_2. Bars = 20 μm. (**F, H**) Quantification of average mucin area/goblet cell ($n = 6$ sample/group; 30–60 cells were quantified/sample) corresponding to experiments performed using *p22 mut* (**E**) and Dynasore-treated wild-type spheroids (**G**). *Atg5VC* and *p22 mut* spheroids were treated with 300 μM H_2O_2 plus or minus 100 μM BAPTA-AM (**I**) or PMA/ionomycin (**J**). (**I, J**) Quantification of average mucin area/goblet cell ($n = 5$ sample/group; 150 cells were quantified/sample). Error bars indicate s.e.m. ****$P < 0.0001$ as determined by the Student's t-test (**I**) or ANOVA with Tukey's multiple post-test comparisons (**J**).

Treatment of BAPTA-AM did not alter autophagic flux (Supplementary Figure S9C). Conversely, we found that release of intracellular calcium stores through treatment with either phorbol myristate acetate (PMA) or ionomycin resulted in diminished intracellular mucin in both Atg5-deficient and *p22 mut* goblet cells, without altering autophagic flux (Figure 7J; Supplementary Figure S9D). Taken together, these results suggested that defects in mucin accumulation associated with loss of function of autophagy proteins and NADPH oxidase components were due to insufficient generation of ROS and cytosolic calcium.

Discussion

Many epithelial secretory cell types require autophagy proteins for their function; however, the mechanistic basis is unclear. In this study, we found that two additional processes, endocytosis and NADPH oxidase-driven ROS production,

work in concert with autophagy proteins to affect goblet cell function. The importance of endocytosis has been demonstrated in many highly secretory cell types (Gundelfinger *et al*, 2003); however, the role of NADPH oxidases is less clear (Crutzen *et al*, 2012; Li *et al*, 2012). In our experiments, inhibition of any one of these three pathways led to the accumulation of mucin in colonic goblet cells that was consistent with decreased secretion. We observed this phenotype using *in vivo* models, as well as a newly developed *in vitro* system to culture and differentiate intestinal epithelial stem cells. In addition, we provided multiple lines of evidence to suggest that these three processes were functionally linked in a common pathway (Figure 8). These processes appeared to intersect at vacuoles that carry both autophagic (LC3) and endocytic (EEA1, Rab7) markers. All three processes were required to maximize the generation of ROS in colonic epithelial cells, and addition of exogenous ROS was sufficient to restore the defect in mucin granule accumulation, supporting the functional linkage of all three components.

We observed in our colonic epithelial cultures that ~70% of LC3 puncta co-localized with the early endosomal marker EEA1. The majority of these vacuoles therefore appear to be amphisomes, formed by fusion between LC3-positive (but, by definition EEA1-negative) autophagosomes and EEA1-positive endosomes. Amphisomes were first characterized more than two decades ago and since then the convergence of endocytosis and autophagy has been noted in several cases (Gordon and Seglen, 1988; Gordon *et al*, 1992; Berg *et al*, 1998; Seglen, 2008; Razi *et al*, 2009). Amphisomes arise from either single or multiple fusion events between autophagosomes and endosomes/phagosomes to form a pre-lysosomal organelle that has been hypothesized to be essential for various cellular processes (Seglen, 2008). Our observation that blockade of endocytosis did not alter LC3 lipidation and puncta formation suggests that inhibition of endocytosis does not inhibit autophagy even when

accumulation of mucins occurs. We found that processes that intersect at these LC3- and EEA1-double positive vacuoles (consistent with amphisomes) were essential for goblet cell function. This finding is important because it potentially links amphisomes to a specific cellular function, in this case the production of ROS, which is required for goblet cell secretion.

Previous observations in phagocytic cells showed that NADPH oxidases are present on endosomes/phagosomes and are important for recruitment of LC3 to phagosomes through LAP (Sanjuan *et al*, 2007; Casbon *et al*, 2009; Huang *et al*, 2009; Henault *et al*, 2012; Lamb *et al*, 2012). In contrast, our findings suggest that LC3 is recruited to amphisomes by a different mechanism that requires conventional autophagy initiating factors such as FIP200 that is not required for LAP. Supporting this, we found that loss of Atg14, another protein required for initiation of the autophagy pathway, also resulted in accumulation of mucin granules. The precise mechanism by which ROS (produced by these NADPH oxidases) regulates cellular functions is often unclear. The downstream effects of ROS are pleotropic in different cell types and include microbial killing, elevation of organelle pH, activation of ion channels, and protein modifications that regulate cell signalling (Bedard and Krause, 2007; Lam *et al*, 2010). Additionally, intracellular ROS can regulate autophagy by altering Atg4 activity (Scherz-Shouval *et al*, 2007). Our findings in colonic goblet cells suggest that ROS can modulate cytosolic calcium levels to regulate mucin granule release.

We found that these amphisome-like vacuoles are a physical site within the goblet cell at which all of the pathways required for goblet cell secretion (autophagy, endocytosis, ROS generation by NADPH oxidases) converge. We therefore propose that these organelles may act as a scaffold in other secretory cell types such as β-islet cells. Interestingly, separate studies in these cells have shown that autophagy proteins (Ebato *et al*, 2008; Jung *et al*, 2008) as well as the
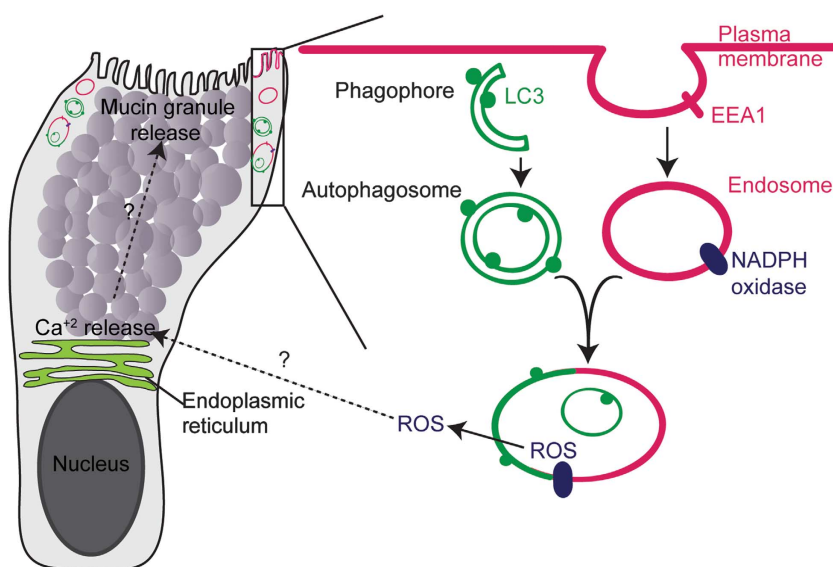
Figure 8 Model of LC3-positive vacuoles that are associated with ROS generation by NADPH oxidases in goblet cells. Schematic of the organelles within a single goblet cell, which are located in the goblet cell cytoplasm in areas distinct from mucin granules (e.g., within the rectangle). An enlarged view of the rectangle contents is included. This area includes the plasma membrane, endosomes, LC3-positive autophagosomes and their fusion product. Endocytosis, autophagosomes and the NADPH oxidase complex are required for the generation of ROS which in turn controls mucin granule accumulation in these cells by as yet unknown mechanisms.

NADPH oxidase (Nox2) regulate insulin secretion (Crutzen et al, 2012; Li et al, 2012); however, these two pathways have not yet been functionally linked in this cell type.

It is interesting that our findings in goblet cells are distinct from what was observed in Paneth cells and osteoclasts. In Paneth cells, loss of autophagy proteins results in abnormal secretory granule morphology and content distribution (Cadwell et al, 2008, 2009, 2010). Here, we observed normal mucin containing granules in goblet cells lacking autophagy proteins. In osteoclasts, secretory lysosomes fuse at the LC3-positive portions of the plasma membrane in an autophagy protein-dependent manner (DeSelm et al, 2011). However, in goblet cells LC3 was localized to amphisomes and was not detected at the plasma membrane. This indicates, remarkably, that while autophagy proteins are required for secretion of granule contents in all three primary cell types, the mechanisms involved appear to be distinct (Cadwell et al, 2008; Marino et al, 2010; DeSelm et al, 2011; Ushio et al, 2011). Primary goblet cells, which can be studied in vivo, in spheroid cultures, and in monolayers proved to be an amenable cell type to uncover unexpected interactions between distinct signalling and trafficking pathways and indicate new avenues of study in other secretory cells that require autophagy protein function.

Materials and methods

Mice
All animal experiments were performed in agreement with protocols approved by the Washington University School of Medicine Animal Studies Committee. Villin-Cre mice were obtained from Jackson Laboratories (Madison et al, 2002). The $Atg5^{flox/flox}$ and $Atg7^{flox/flox}$ mice and the breeding scheme to generate $Atg5VC$, $Atg7VC$ and littermate controls were described previously (Hara et al, 2006; Cadwell et al, 2008). $LC3\beta^{-/-}$, $FIP200^{flox/flox}$, $Atg14^{flox/flox}$, $Cyba^{nmf333/nmf333}$ ($p22phox$ mutant) and $p47phox^{-/-}$ mice were previously described (Jackson et al, 1995; Gan et al, 2006; Cann et al, 2008; Nakano et al, 2008; Matsunaga et al, 2009). For NAC experiments, drinking water with 3% NAC (or without NAC as a control) was changed every 48 h for the 7-day treatment period. Mice were housed in a specific pathogen-free barrier facility with the addition of screening for Murine Norovirus, and were maintained under a strict 12-h light cycle and fed autoclaved chow diet (PicoLab Rodent Chow 20, Purina Mills).

Intestinal epithelial culture
Colonic crypts were isolated and cultured in Matrigel (BD Biosciences) in the presence of 50% conditioned medium (CM) containing Wnt3a, R-spondin 3 and Noggin. This method generated epithelial spheroids enriched for Lrg5-positive stem cells (Miyoshi et al, 2012). To induce goblet cell differentiation, spheroids were incubated in 5% CM plus 5 µM DAPT (Sigma). Lipopolysaccharides (LPSs) from E. coli (Sigma) were dissolved in PBS at 1 mg/ml and added to cultures at a final concentration of 25 µg/ml for final the 48 h of the culture period. DPI chloride (Sigma) was dissolved in DMSO and administered at a final concentration of 10 µM for 4 h. Dynasore (EMD Chemicals) was dissolved in DMSO and administered to cultures at a final concentration of 100 µM for 1 h. Hydrogen peroxide (Sigma) was diluted in sterile water and added to cultures at a final concentration of 300 µM for 1 h. BAPTA-AM (Abcam) was dissolved in DMSO and added to cultures at a final concentration of 100 µM for 1 h. PMA and ionomycin (Sigma) were dissolved in DMSO and added to cultures at a final concentration of 1 µM and 100 nM, respectively. For 2D cultures, spheroids were trypsinized and passed through a 70-µm filter. Approximately 4000 aggregates per well were plated onto a Matrigel-coated (1:40 dilution of Matrigel in PBS was used for coating) 8-well chambered slide (Nunc). During seeding, ROCK inhibitor (Y-27632, Sigma) was added at a final concentration of 10 µM. After 24 h, 5% CM plus 5 µM DAPT was used for a culture period of 3 days to obtain differentiated cells.

For Tat-Cre mediated recombination, 5 µM Tat-Cre protein was added to a single-cell suspension of colonic epithelial cells obtained from colonic spheroids in 50% CM with 10 µM Y-27632 overnight (Morimoto et al, 2010; Shaw et al, 2008). The next day the cells were pelleted, plated in matrigel, and cultured as described above. Single spheroids were picked and genotyped to determine recombination efficiency.

Histology
Colons were removed, cut open along the proximal-distal axis and pinned flat. The tissue was incubated in Bouin's fixative for 16 h at 4°C, and then blocked in 2% blocking agar for paraffin embedment. In all, 5 µm sections were stained with Alcian Blue, Periodic acid-Schiff (PAS) or Haematoxylin and Eosin. Images were captured at room temperature using an Olympus BX51 microscope, which was equipped with a 40 × (0.75 NA) UPlan FL air objective. Image preparation and adjustment of brightness and contrast of images were done using Adobe Photoshop CS3.

Immunofluorescence
All images were captured at room temperature using a Zeiss Axiovert 200 with Axiocam MRM camera and AxioVision software. The follow objectives on the microscope were used for image acquisition: a 20 × (0.8 NA) Plan-APOCHROMAT air objective (for visualization of whole-mount tissue and spheroids), and a 40 × (1.3 NA) Plan-NEOFLUAR oil objective (for visualization of colonic epithelial cells). For whole-mount immunofluorescence, colons were dissected, carefully opened lengthwise, pinned flat, and fixed in 10% buffered formalin for 1 h at 24°C without disrupting the luminal contents. The tissue was rinsed three times in PBS and stained with 1:100 TRITC-conjugated lectin from Ulex europaeus (UEA, Sigma) for 1 h at 24°C. The tissue was then counterstained with bis-benzimide to label nuclei and mounted on glass slides using Mowiol media. Images were taken at a magnification of × 20. For immunohistochemistry, formalin-fixed paraffin-embedded tissue sections were de-paraffinized using standard procedures and antigen retrieved with Trilogy buffer (Cell Marque). Sections were blocked in 1% BSA, 0.3% Triton X-100 PBS and incubated with the respective antibodies overnight at 4°C (1:100 dilution). Mouse monoclonal anti-LC3 was from MBL international (M152-3B). Sections were then incubated with Alexa488-conjugated anti-mouse secondary antibody for 1 h at room temperature. Followed by counterstain with bis-benzimide and coverslipped with a 1:1 glycerol/PBS solution. For immunofluorescence detection of goblet cells in crypt cultures, spheroids were grown on chambered slides (Nunc) and fixed in methanol. Mucin was detected using either a Rabbit polyclonal anti-Mucin2 (H-300) (Santa Cruz, sc-15334) or a TRITC-conjugated lectin from UEA (Sigma). Secondary antibody was an Alexa488-conjugated anti-rabbit antibody (Invitrogen). Staining and visualization were performed as described for tissue sections. For immunocytochemistry of colonic epithelial cells, monolayers were grown on Matrigel-coated glass chambered slides and fixed with 4% PFA for 15 min. Cells were blocked in 1% BSA, 0.1% Triton X-100 PBS with addition of 10% donkey serum and incubated with the respective antibodies overnight at 4°C (1:100 dilution). Rabbit LC3B was from Sigma (L7543), and Goat EEA1 and p22phox were from Santa Cruz (sc-6414 and sc-11712). Secondary staining was performed using Alexa488-conjugated anti-rabbit antibody and Alexa594-conjugated anti-goat antibodies (Invitrogen). Visualization was performed as described for tissue sections. Image preparation and adjustment of brightness and contrast of images were done using Adobe Photoshop CS3.

Immunoblotting and autophagy flux assays
Differentiated colonic spheroids were isolated using Cell Recovery Media (BD Biosciences) to remove matrigel. For flux assays, organoids were treated with 100 nM bafilomycin A1 (Sigma) for 1 h in the presence of indicated drugs. Spheroids were then pelleted and lysed in RIPA buffer with protease inhibitors (Sigma). Samples were run on 15% Tris–HCl gels (Bio-Rad) and transferred onto nitrocellulose membrane (Bio-Rad). Membranes were blocked with 5% milk in 0.1% Tween-20 Tris-buffered saline for 1 h at room temperature and probed with the antibodies: rabbit anit-LC3 (Sigma), mouse anti-GAPDH, and goat anit-p22phox (Santa Cruz

Biotechnology) overnight at 4°C. Blots were incubated for 1 h with horseradish peroxidase-conjugated secondary antibodies (Sigma) before development using the SuperSignal West Dura chemiluminescent kit (Thermo Fisher Scientific).

LCM and microarray analysis

LCM and RNA isolation techniques from mouse colon were performed as previously described (Stappenbeck et al, 2003; Pull et al, 2005). Briefly, colons were removed, infused with OCT and frozen. In all, 6 μm serial sections were cut and stained with methyl green. The goblet cells residing in the lower crypts of the descending colon were captured and total RNA was isolated. Total cellular RNA was extracted (PicoPure RNA isolation kit; Arcturus).

Preparation and analysis of Agilent whole mouse genome arrays

In all, 5 ng of total RNA from each sample was amplified using the Transplex Complete Whole Transcriptome Amplification Kit (Sigma), labelled using a modified protocol with the ULS aRNA Fluorescent Cy5 labeling kit (Kreatech Diagnostics); and purified using DNA Clean and Concentrate spin columns according to the manufacturer's protocol (Zymo Research Corporation). cDNA was hybridized to 4×44K Mouse Whole Genome Microarrays (Agilent) for 18 h following the manufacturer's protocol. Microarrays were washed in $0.01 \times$ SSC/0.005% Triton X-102 at 40°C, dried with HEPA filtered compressed nitrogen and scanned on an Agilent Technologies DNA Microarray Scanner at 5 μm resolution. Data were extracted from the scanned image using the Agilent Technologies Feature Extraction Software, background subtracted, and normalized by the Lowess method (Yang et al, 2002). The fold increase or decrease in mRNA expression was calculated by comparing the Atg5VC to control. GO term and KEGG pathway analysis of significantly changed genes were analysed using the DAVID Bioinformatics tool (Huang da et al, 2009a, b).

ROS and calcium detection

Crypt cultures were grown on 24-well plates and treated as described in various experiments. Cells were washed in HBSS and incubated with 5 μM of fluorescent ROS indicator 5-(and-6)-chloromethyl-2′,7′-dichlorodihydrofluorescein diacetate, acetyl ester (DCF) (Invitrogen) for 15 min. After incubation, crypt cultures were washed in HBSS three times. Images for quantification were captured with a Zeiss Axiovert 200 with Axiocam MRM camera with a $\times 10$ objective. To minimize effects of photo-oxidation, a maximum of four wells were imaged per experiment.

For calcium detection assays, cells were washed in HBSS and incubated with 5 μM Fluo-4 (Invitrogen) for 30 min. Cells were then washed in HBSS and the dye was allowed to equilibrate for 30 min. Images were captured as described above.

qRT–PCR analysis

RNA from crypt cultures was isolated and purified using the NucleoSpin RNA II extraction kit (Machery-Nagel) according to the manufacturer's protocol. For cDNA synthesis, Superscript reverse transcriptase and random primers were used (Invitrogen). qRT-PCR was performed in triplicate for each sample using SYBR-Green master mix (Clontech) and analysed by Eppendorf Realplex Mastercycler.

Quantification and statistical analysis

Quantification of goblet cell theca size, and ROS production by DCF was conducted using the ImageJ software (NIH). LC3 and EEA1 colocalization was conducted using the co-localization plug-in for ImageJ. Statistical significance between groups was determined using either Student's t-tests or ANOVA in Prism GraphPad Software.

Electron microscopy

For transmission electron microscopy, 1 cm^2 tissue was dissected from ascending and transverse colons of control and Atg5VC mice. Samples were fixed in 2% paraformaldehyde, 2% glutaraldehyde and prepared for electron microscopy. Sections were viewed with a JEOL model 100C electron microscope. For immunogold electron microscopy, colonic tissue was fixed in 4% paraformaldehyde/0.05% glutaraldehyde (Polysciences Inc.) in 100 mM PIPES/0.5 mM $MgCl_2$, pH 7.2 for 1 h at 4°C and incubated overnight in the cryoprotectant 2.3 M sucrose/20% polyvinyl pyrrolidone in PIPES/$MgCl_2$ at 4°C. Samples were probed with the mouse monoclonal anti-LC3 (MBL), anti-p22phox (Santa Cruz), anti-EEA1 (Santa Cruz), anti-Rab5 (Cell Signaling), anti-Rab7 (Cell Signaling), Rab11 (Cell Signaling, and Lamp1 (Santa Cruz) at a 1:50 dilution and viewed on a JEOL 1200 EX transmission electron microscope (JEOL USA Inc.).

Cerium chloride precipitation for ROS localization

Visualization of ROS production by cerium chloride precipitation method was performed as previously described (Vazquez-Torres et al, 2000; Lam et al, 2011). Briefly, differentiated colonic spheroids were trypsinized and plated on transwells and cells were washed with 0.1 M Tris maleate buffer, pH 7.5 at 37°C, followed by the addition of 0.1 M Tris maleate, 7% sucrose (Sigma), 1 mM aminotriazole buffer, pH 7.5 for 10 min at 37°C. Next, cells were treated with 0.1 M Tris maleate, 7% sucrose, 1 mM aminotriazole, 1 mM $CeCl_3$, 0.71 mM NADH, 0.71 mM NADPH buffer pH 7.5 for 20 min at 37°C (Sigma). Cells were then washed with 0.1 M Tris maleate, 7% sucrose and fixed in 2.5% glutaraldehyde in PBS overnight, postfixed in 1% OsO_4, stained with 1% aqueous uranyl acetate, dehydrated in graded series of ethanols and embedded in epoxy resin. Samples were then sectioned, stained with 2% uranyl acetate, then 0.2% lead citrate, and viewed on a JEOL 1200 EX transmission electron microscope (JEOL USA Inc.).

Supplementary data

Supplementary data are available at The EMBO Journal Online (http://www.embojournal.org).

Acknowledgements

Conflict of interest

The authors declare that they have no conflict of interest.

References

Abdullah LH, Conway JD, Cohn JA, Davis CW (1997) Protein kinase C and Ca2 + activation of mucin secretion in airway goblet cells. Am J Physiol 273: L201–L210

Anderson CA, Boucher G, Lees CW, Franke A, D'Amato M, Taylor KD, Lee JC, Goyette P, Imielinski M, Latiano A, Lagace C, Scott R, Amininejad L, Bumpstead S, Baidoo L, Baldassano RN, Barclay M, Bayless TM, Brand S, Buning C et al (2011) Meta-analysis identifies 29 additional ulcerative colitis risk loci, increasing the number of confirmed associations to 47. Nat Genet 43: 246–252

Artis D, Grencis RK (2008) The intestinal epithelium: sensors to effectors in nematode infection. Mucosal Immunol 1: 252–264

Bedard K, Krause KH (2007) The NOX family of ROS-generating NADPH oxidases: physiology and pathophysiology. Physiol Rev 87: 245–313

Berg TO, Fengsrud M, Stromhaug PE, Berg T, Seglen PO (1998) Isolation and characterization of rat liver amphisomes. Evidence for fusion of autophagosomes with both early and late endosomes. *J Biol Chem* **273:** 21883–21892

Cadwell K, Liu JY, Brown SL, Miyoshi H, Loh J, Lennerz JK, Kishi C, Kc W, Carrero JA, Hunt S, Stone CD, Brunt EM, Xavier RJ, Sleckman BP, Li E, Mizushima N, Stappenbeck TS, Virgin 4th HW (2008) A key role for autophagy and the autophagy gene Atg16l1 in mouse and human intestinal Paneth cells. *Nature* **456:** 259–263

Cadwell K, Patel KK, Komatsu M, Virgin 4th HW, Stappenbeck TS (2009) A common role for Atg16L1, Atg5 and Atg7 in small intestinal Paneth cells and Crohn disease. *Autophagy* **5:** 250–252

Cadwell K, Patel KK, Maloney NS, Liu TC, Ng AC, Storer CE, Head RD, Xavier R, Stappenbeck TS, Virgin HW (2010) Virus-plus-susceptibility gene interaction determines Crohn's disease gene Atg16L1 phenotypes in intestine. *Cell* **141:** 1135–1145

Cann GM, Guignabert C, Ying L, Deshpande N, Bekker JM, Wang L, Zhou B, Rabinovitch M (2008) Developmental expression of LC3alpha and beta: absence of fibronectin or autophagy phenotype in LC3beta knockout mice. *Dev Dyn* **237:** 187–195

Casbon AJ, Allen LA, Dunn KW, Dinauer MC (2009) Macrophage NADPH oxidase flavocytochrome B localizes to the plasma membrane and Rab11-positive recycling endosomes. *J Immunol* **182:** 2325–2339

Chang WW, Leblond CP (1971) Renewal of the epithelium in the descending colon of the mouse. I. Presence of three cell populations: vacuolated-columnar, mucous and argentaffin. *Am J Anat* **131:** 73–99

Cheranov SY, Jaggar JH (2006) TNF-alpha dilates cerebral arteries via NAD(P)H oxidase-dependent Ca2+ spark activation. *Am J Physiol Cell Physiol* **290:** C964–C971

Conway JD, Bartolotta T, Abdullah LH, Davis CW (2003) Regulation of mucin secretion from human bronchial epithelial cells grown in murine hosted xenografts. *Am J Physiol Lung Cell Mol Physiol* **284:** L945–L954

Crutzen R, Shlyonsky V, Louchami K, Virreira M, Hupkens E, Boom A, Sener A, Malaisse WJ, Beauwens R (2012) Does NAD(P)H oxidase-derived H2O2 participate in hypotonicity-induced insulin release by activating VRAC in beta-cells? *Pflugers Arch* **463:** 377–390

Davis CW, Dickey BF (2008) Regulated airway goblet cell mucin secretion. *Annu Rev Physiol* **70:** 487–512

DeSelm CJ, Miller BC, Zou W, Beatty WL, van Meel E, Takahata Y, Klumperman J, Tooze SA, Teitelbaum SL, Virgin HW (2011) Autophagy proteins regulate the secretory component of osteoclastic bone resorption. *Dev Cell* **21:** 966–974

Ebato C, Uchida T, Arakawa M, Komatsu M, Ueno T, Komiya K, Azuma K, Hirose T, Tanaka K, Kominami E, Kawamori R, Fujitani Y, Watada H (2008) Autophagy is important in islet homeostasis and compensatory increase of beta cell mass in response to high-fat diet. *Cell Metab* **8:** 325–332

Falk P, Roth KA, Gordon JI (1994) Lectins are sensitive tools for defining the differentiation programs of mouse gut epithelial cell lineages. *Am J Physiol* **266:** G987–G1003

Florey O, Kim SE, Sandoval CP, Haynes CM, Overholtzer M (2011) Autophagy machinery mediates macroendocytic processing and entotic cell death by targeting single membranes. *Nat Cell Biol* **13:** 1335–1343

Franke A, McGovern DP, Barrett JC, Wang K, Radford-Smith GL, Ahmad T, Lees CW, Balschun T, Lee J, Roberts R, Anderson CA, Bis JC, Bumpstead S, Ellinghaus D, Festen EM, Georges M, Green T, Haritunians T, Jostins L, Latiano A *et al* (2010) Genome-wide meta-analysis increases to 71 the number of confirmed Crohn's disease susceptibility loci. *Nat Genet* **42:** 1118–1125

Gan B, Peng X, Nagy T, Alcaraz A, Gu H, Guan JL (2006) Role of FIP200 in cardiac and liver development and its regulation of TNFalpha and TSC-mTOR signaling pathways. *J Cell Biol* **175:** 121–133

Gordon PB, Hoyvik H, Seglen PO (1992) Prelysosomal and lysosomal connections between autophagy and endocytosis. *Biochem J* **283:** 361–369

Gordon PB, Seglen PO (1988) Prelysosomal convergence of autophagic and endocytic pathways. *Biochem Biophys Res Commun* **151:** 40–47

Granados MP, Salido GM, Gonzalez A, Pariente JA (2006) Dose-dependent effect of hydrogen peroxide on calcium mobilization in mouse pancreatic acinar cells. *Biochem Cell Biol* **84:** 39–48

Gundelfinger ED, Kessels MM, Qualmann B (2003) Temporal and spatial coordination of exocytosis and endocytosis. *Nat Rev Mol Cell Biol* **4:** 127–139

Hara T, Nakamura K, Matsui M, Yamamoto A, Nakahara Y, Suzuki-Migishima R, Yokoyama M, Mishima K, Saito I, Okano H, Mizushima N (2006) Suppression of basal autophagy in neural cells causes neurodegenerative disease in mice. *Nature* **441:** 885–889

Henault J, Martinez J, Riggs JM, Tian J, Mehta P, Clarke L, Sasai M, Latz E, Brinkmann MM, Iwasaki A, Coyle AJ, Kolbeck R, Green DR, Sanjuan MA (2012) Noncanonical autophagy is required for type I interferon secretion in response to DNA-immune complexes. *Immunity* **37:** 986–997

Hidalgo C, Sanchez G, Barrientos G, Aracena-Parks P (2006) A transverse tubule NADPH oxidase activity stimulates calcium release from isolated triads via ryanodine receptor type 1 S - glutathionylation. *J Biol Chem* **281:** 26473–26482

Huang J, Canadien V, Lam GY, Steinberg BE, Dinauer MC, Magalhaes MA, Glogauer M, Grinstein S, Brumell JH (2009) Activation of antibacterial autophagy by NADPH oxidases. *Proc Natl Acad Sci USA* **106:** 6226–6231

Huang da W, Sherman BT, Lempicki RA (2009a) Bioinformatics enrichment tools: paths toward the comprehensive functional analysis of large gene lists. *Nucleic Acids Res* **37:** 1–13

Huang da W, Sherman BT, Lempicki RA (2009b) Systematic and integrative analysis of large gene lists using DAVID bioinformatics resources. *Nat Protoc* **4:** 44–57

Jackson SH, Gallin JI, Holland SM (1995) The p47phox mouse knock-out model of chronic granulomatous disease. *J Exp Med* **182:** 751–758

Johansson ME, Larsson JM, Hansson GC (2011) The two mucus layers of colon are organized by the MUC2 mucin, whereas the outer layer is a legislator of host-microbial interactions. *Proc Natl Acad Sci USA* **108**(Suppl 1): 4659–4665

Jung HS, Chung KW, Won Kim J, Kim J, Komatsu M, Tanaka K, Nguyen YH, Kang TM, Yoon KH, Kim JW, Jeong YT, Han MS, Lee MK, Kim KW, Shin J, Lee MS (2008) Loss of autophagy diminishes pancreatic beta cell mass and function with resultant hyperglycemia. *Cell Metab* **8:** 318–324

Komatsu M, Waguri S, Ueno T, Iwata J, Murata S, Tanida I, Ezaki J, Mizushima N, Ohsumi Y, Uchiyama Y, Kominami E, Tanaka K, Chiba T (2005) Impairment of starvation-induced and constitutive autophagy in Atg7-deficient mice. *J Cell Biol* **169:** 425–434

Lam GY, Fattouh R, Muise AM, Grinstein S, Higgins DE, Brumell JH (2011) Listeriolysin O suppresses phospholipase C-mediated activation of the microbicidal NADPH oxidase to promote Listeria monocytogenes infection. *Cell Host Microbe* **10:** 627–634

Lam GY, Huang J, Brumell JH (2010) The many roles of NOX2 NADPH oxidase-derived ROS in immunity. *Semin Immunopathol* **32:** 415–430

Lamb FS, Hook JS, Hilkin BM, Huber JN, Volk AP, Moreland JG (2012) Endotoxin priming of neutrophils requires endocytosis and NADPH oxidase-dependent endosomal reactive oxygen species. *J Biol Chem* **287:** 12395–12404

Levine B, Mizushima N, Virgin HW (2011) Autophagy in immunity and inflammation. *Nature* **469:** 323–335

Li N, Li B, Brun T, Deffert-Delbouille C, Mahiout Z, Daali Y, Ma XJ, Krause KH, Maechler P (2012) NADPH oxidase NOX2 defines a new antagonistic role for reactive oxygen species and cAMP/PKA in the regulation of insulin secretion. *Diabetes* **61:** 2842–2850

Longatti A, Lamb CA, Razi M, Yoshimura S, Barr FA, Tooze SA (2012) TBC1D14 regulates autophagosome formation via Rab11- and ULK1-positive recycling endosomes. *J Cell Biol* **197:** 659–675

Madison BB, Dunbar L, Qiao XT, Braunstein K, Braunstein E, Gumucio DL (2002) Cis elements of the villin gene control expression in restricted domains of the vertical (crypt) and horizontal (duodenum, cecum) axes of the intestine. *J Biol Chem* **277:** 33275–33283

Marino G, Fernandez AF, Cabrera S, Lundberg YW, Cabanillas R, Rodriguez F, Salvador-Montoliu N, Vega JA, Germana A, Fueyo A, Freije JM, Lopez-Otin C (2010) Autophagy is essential for mouse sense of balance. *J Clin Invest* **120:** 2331–2344

Martinez J, Almendinger J, Oberst A, Ness R, Dillon CP, Fitzgerald P, Hengartner MO, Green DR (2011) Microtubule-associated protein 1 light chain 3 alpha (LC3)-associated phagocytosis is required for the efficient clearance of dead cells. *Proc Natl Acad Sci USA* **108:** 17396–17401

Matsunaga K, Saitoh T, Tabata K, Omori H, Satoh T, Kurotori N, Maejima I, Shirahama-Noda K, Ichimura T, Isobe T, Akira S, Noda T, Yoshimori T (2009) Two Beclin 1-binding proteins, Atg14L and Rubicon, reciprocally regulate autophagy at different stages. *Nat Cell Biol* **11:** 385–396

McGuckin MA, Linden SK, Sutton P, Florin TH (2011) Mucin dynamics and enteric pathogens. *Nat Rev Microbiol* **9:** 265–278

Miyoshi H, Ajima R, Luo CT, Yamaguchi TP, Stappenbeck TS (2012) Wnt5a potentiates TGF-beta signaling to promote colonic crypt regeneration after tissue injury. *Science* **338:** 108–113

Morimoto M, Liu Z, Cheng HT, Winters N, Bader D, Kopan R (2010) Canonical Notch signaling in the developing lung is required for determination of arterial smooth muscle cells and selection of Clara versus ciliated cell fate. *J Cell Sci* **123:** 213–224

Nakano Y, Longo-Guess CM, Bergstrom DE, Nauseef WM, Jones SM, Banfi B (2008) Mutation of the Cyba gene encoding p22phox causes vestibular and immune defects in mice. *J Clin Invest* **118:** 1176–1185

Pellegrinet L, Rodilla V, Liu Z, Chen S, Koch U, Espinosa L, Kaestner KH, Kopan R, Lewis J, Radtke F (2011) Dll1- and dll4-mediated notch signaling are required for homeostasis of intestinal stem cells. *Gastroenterology* **140:** 1230–1240 e1231–1237

Pull SL, Doherty JM, Mills JC, Gordon JI, Stappenbeck TS (2005) Activated macrophages are an adaptive element of the colonic epithelial progenitor niche necessary for regenerative responses to injury. *Proc Natl Acad Sci USA* **102:** 99–104

Ravikumar B, Moreau K, Jahreiss L, Puri C, Rubinsztein DC (2010) Plasma membrane contributes to the formation of pre-autophagosomal structures. *Nat Cell Biol* **12:** 747–757

Razi M, Chan EY, Tooze SA (2009) Early endosomes and endosomal coatomer are required for autophagy. *J Cell Biol* **185:** 305–321

Sanjuan MA, Dillon CP, Tait SW, Moshiach S, Dorsey F, Connell S, Komatsu M, Tanaka K, Cleveland JL, Withoff S, Green DR (2007) Toll-like receptor signalling in macrophages links the autophagy pathway to phagocytosis. *Nature* **450:** 1253–1257

Scherz-Shouval R, Shvets E, Fass E, Shorer H, Gil L, Elazar Z (2007) Reactive oxygen species are essential for autophagy and specifically regulate the activity of Atg4. *EMBO J* **26:** 1749–1760

Seglen PO (2008) Where endocytosis and autophagy meet: The amphisome. In *Hepatic Endocytosis*, Sporstol Fonhus M, Mousavi SA, Berg T (eds), pp 61–100. Trivandrum (Kerala): Transworld Research Network

Shaw PA, Catchpole IR, Goddard CA, Colledge WH (2008) Comparison of protein transduction domains in mediating cell delivery of a secreted CRE protein. *Biochemistry* **47:** 1157–1166

Snippert HJ, van der Flier LG, Sato T, van Es JH, van den Born M, Kroon-Veenboer C, Barker N, Klein AM, van Rheenen J, Simons BD, Clevers H (2010) Intestinal crypt homeostasis results from neutral competition between symmetrically dividing Lgr5 stem cells. *Cell* **143:** 134–144

Specian RD, Oliver MG (1991) Functional biology of intestinal goblet cells. *Am J Physiol* **260:** C183–C193

Stappenbeck TS, Mills JC, Gordon JI (2003) Molecular features of adult mouse small intestinal epithelial progenitors. *Proc Natl Acad Sci USA* **100:** 1004–1009

Ushio H, Ueno T, Kojima Y, Komatsu M, Tanaka S, Yamamoto A, Ichimura Y, Ezaki J, Nishida K, Komazawa-Sakon S, Niyonsaba F, Ishii T, Yanagawa T, Kominami E, Ogawa H, Okumura K, Nakano H (2011) Crucial role for autophagy in degranulation of mast cells. *J Allergy Clin Immunol* **127:** 1267–1276 e1266

Vazquez-Torres A, Xu Y, Jones-Carson J, Holden DW, Lucia SM, Dinauer MC, Mastroeni P, Fang FC (2000) Salmonella pathogenicity island 2-dependent evasion of the phagocyte NADPH oxidase. *Science* **287:** 1655–1658

Wang X, Takeda S, Mochizuki S, Jindal R, Dhalla NS (1999) Mechanisms of hydrogen peroxide-induced increase in intracellular calcium in cardiomyocytes. *J Cardiovasc Pharmacol Ther* **4:** 41–48

Yang YH, Dudoit S, Luu P, Lin DM, Peng V, Ngai J, Speed TP (2002) Normalization for cDNA microarray data: a robust composite method addressing single and multiple slide systematic variation. *Nucleic Acids Res* **30:** e15

Zhu Y, Ehre C, Abdullah LH, Sheehan JK, Roy M, Evans CM, Dickey BF, Davis CW (2008) Munc13-2-/- baseline secretion defect reveals source of oligomeric mucins in mouse airways. *J Physiol* **586:** 1977–1992